$42^{nd}$ **AIAA Aerospace Sciences Meeting and Exhibit**
**5-8 January 2004, Reno, Nevada**

**AIAA-2004-0698**

# AIRFRAME NOISE MODELING APPROPRIATE FOR MULTIDISCIPLINARY DESIGN AND OPTIMIZATION

Serhat Hosder*, Joseph A. Schetz†, Bernard Grossman‡, and William H. Mason§

*Virginia Polytechnic Institute and State University*
*Blacksburg, VA 24061-0203*

## Abstract

A Trailing Edge Noise Metric has been developed for constructing response surfaces that may be used for optimization problems involving aerodynamic noise from a clean wing. The modeling approach includes a modified version of a theoretical trailing edge noise prediction and utilizes a high fidelity CFD (RANS) code with a two-equation turbulence model to obtain the characteristic velocity and length scales used in the noise model. The noise metric is not the absolute value of the noise intensity, but an accurate relative noise measure as shown in the validation studies. Parametric studies were performed to investigate the effect of the wing geometry and the lift coefficient on the noise metric. 2-D parametric studies were done using two subsonic (NACA0012 and NACA0009) and two supercritical (SC(2)-0710 and SC(2)-0714) airfoils. The EET Wing (a generic conventional transport wing) was used for the 3-D study. With NACA 0012 and NACA 0009 airfoils, a reduction in the trailing edge noise was obtained by decreasing the lift coefficient and the thickness ratio, while increasing the chord length to keep the same lift at a constant speed. Supercritical airfoil studies showed that decreasing the thickness ratio may increase the noise at high lift coefficients while a reduction may be obtained at low lift coefficients. Both 2-D and 3-D studies demonstrated that the trailing edge noise remains almost constant at low lift coefficients and gets larger at high lift coefficients. The increase in the noise metric can be dramatic when there is significant flow separation. Three-dimensional effects observed in the EET Wing case indicate the importance of calculating the noise metric with a characteristic velocity and length scale that vary along the span.

*Graduate student, Department of Aerospace and Ocean Engineering, Student Member AIAA

†Fred D. Durham Endowed Chair, Department of Aerospace and Ocean Engineering, Fellow AIAA

‡Professor, Department of Aerospace and Ocean Engineering. Currently Vice President, Education and Outreach, National Institute of Aerospace, Hampton, VA. Fellow AIAA

§Professor, Department of Aerospace and Ocean Engineering, Associate Fellow AIAA



## Nomenclature

| | |
|---|---|
| $a_\infty$ | = free-stream speed of sound |
| $b$ | = wing span |
| $c$ | = chord |
| $c_a$ | = mean geometric chord |
| $c_f$ | = skin friction coefficient |
| $C_d$ | = section drag coefficient |
| $C_D$ | = overall drag coefficient |
| $C_l$ | = section lift coefficient |
| $C_L$ | = overall lift coefficient |
| $D$ | = directivity function |
| $H$ | = distance to the ground or receiver |
| $I$ | = noise intensity |
| $I_{NM}$ | = noise intensity indicator |
| $l_0$ | = characteristic length scale for turbulence |
| $mac$ | = mean aerodynamic chord |
| $NM$ | = noise metric |
| $NM_{upper}$ | = noise metric for wing upper surface |
| $NM_{lower}$ | = noise metric for wing lower surface |
| $OASPL$ | = overall sound pressure level |
| $Re_{mac}$ | = Reynolds number based on $mac$ |
| $Re_c$ | = Reynolds number based on chord |
| $SPL$ | = sound pressure level |
| $S_{ref}$ | = wing reference area |
| $t/c$ | = thickness ratio |
| $TKE$ | = turbulent kinetic energy |
| $u_0$ | = characteristic velocity scale for turbulence |
| $V_\infty$ | = free-stream velocity |
| $\alpha$ | = angle of attack |
| $\beta$ | = trailing edge sweep angle |
| $\omega$ | = turbulence frequency |
| $\omega_0$ | = characteristic source frequency |
| $\psi$ | = azimuthal directivity angle |
| $\rho_\infty$ | = free-stream density |
| $\theta$ | = polar directivity angle |

## Introduction

Aircraft noise has become an important performance criterion and constraint in aircraft design in recent years. Although there has been a dramatic reduction in the aircraft noise in the last three decades with the advances in airframe and engine technology, further reduction is still needed to allow civil aviation to grow and to minimize noise pollution. Aircraft

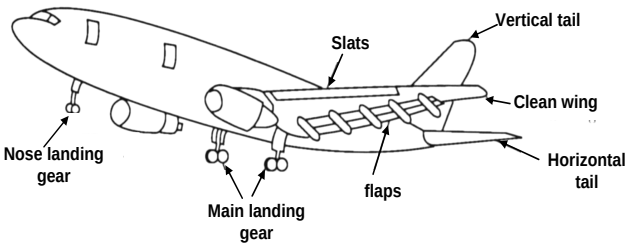


Figure 1: **Airframe noise sources (from Crighton[4])**

noise regulations curtails the growth of air transportation. These regulations limit the hours and the number of operations at most airports and impede aviation infrastructure improvements such as airport expansion and construction plans.[1] There has been almost a 100% increase in the number of noise related restrictions in the last decade.[2] The goal of *10 dB noise reduction in 10 years* was set by NASA[3] in 1997 to tackle the aircraft noise problem and its negative impact on the future of civil aviation. To achieve this challenging noise reduction goal, research efforts have been focused on: (1) the design of revolutionary aircraft with innovative configurations and technologies to give the minimum noise signature (2) the improvement of conventional aircraft noise performance, and (3) optimizing the flight performance parameters or operational conditions for minimum noise. All these efforts clearly require addressing noise in the aircraft conceptual design phase.

Engine noise, engine/airframe interference noise, and airframe noise are the main components of aircraft noise. The noise radiating from each component covers a different fraction of the total noise at different flight regimes. At take off, the dominant noise source is the engine. However, the use of high-bypass ratio turbofan engines and other achievements in engine technology make the airframe noise level comparable to the engine noise at approach conditions. To include aircraft noise as a constraint or an objective function in a Multidisciplinary Design and Optimization (MDO) framework, each noise component should be modeled. These models are required to predict the aircraft noise originating from different sources in different flight regimes.

Airframe noise is defined as the *non-propulsive* noise of an aircraft in flight.[4] Airframe noise sources on a conventional transport are the landing gear, trailing edge flaps, leading edge slats, the *clean* wing, and tail surfaces[5] (Figure 1). A *clean* wing has all its high-lift devices and the undercarriage in stowed position. The main noise mechanism of a clean wing is the Trailing Edge (TE) Noise. The landing gear, flaps and slats are the dominant airframe noise sources for an airplane at the approach before landing. However,

- Trailing Edge Noise can be a significant contributor to the airframe noise for a non-conventional configuration that does not use traditional high-lift devices on approach such as a Blended-Wing-Body (BWB) transport aircraft, which has a large wing area and span, a conventional aircraft or a BWB with distributed propulsion[6,7] that uses the jet-wing concept for high-lift, or an airplane with a morphing wing.

- A Trailing Edge Noise formulation based on proper physics may also be used to predict the noise originating from the flap trailing-edges and flap-side edges at high lift conditions.

- Trailing Edge Noise of a clean wing at high lift can be thought as a *lower bound* value of the airframe noise on approach. In other words, if we can obtain the same lift required at the approach without using the traditional high-lift devices, the noise of the clean wing would be the lowest value that can be achieved for that particular aircraft as long as there is no large region of flow separation on the wing. This value can be used as a measure of merit in noise reduction studies.

In this paper, we have focused on airframe noise modeling for a clean wing at approach conditions. Our objective has been to develop a *noise metric* for constructing response surfaces that may be used in the optimization of a clean wing for minimum noise. We investigate the effect of wing geometry (thickness ratio, $t/c$, of wing sections, and the chord length $c$) and the lift coefficient on the noise metric by performing parametric studies. Two-dimensional parametric studies were done using subsonic and supercritical airfoils. A generic conventional transport wing was used for the three-dimensional studies.

We expect our noise metric to be a reliable indicator of airframe noise, but not necessarily the magnitude of the absolute noise signature. It should also be relatively inexpensive to calculate. However, we still use 3-D, Reynolds-Averaged-Navier-Stokes (RANS) calculations in our approach. Our methodology for obtaining the noise metric on a clean wing includes a modified version of the theoretical trailing edge noise prediction models given in Goldstein[8] and Lilley.[5,9] We use a high fidelity CFD (RANS) code with a two-equation turbulence model to obtain the characteristic velocity and length scales that are used in the new noise metric developed here.

## Clean Wing Noise Modeling

The noise originating from the interaction of the turbulent flow with a sharp-edged body such as the trailing edge of a wing or a flap has been one of the main research areas of aeroacoustics for many years. Howe[10] gives a review of various trailing edge noise theories and lists them in different categories. Most of the theories used in predicting the trailing edge noise are based on Lighthill's Acoustic Analogy.[11] Ffowcs-Williams and Hall[12] were the first to solve the problem of noise radiated from the turbulent flow past a semi-infinite plate of zero thickness at zero angle of attack using this analogy. The trailing edge noise originates from scattering of the acoustic waves generated due to the passage of the turbulent boundary layers over the trailing edge of wings or flaps.[5] All theories on trailing edge noise show that the noise intensity varies approximately with the $5^{th}$ power of the free-stream velocity.[4,10] It is also proportional to the trailing-edge length along the span and a characteristic length scale for turbulence.

Most of the trailing edge noise prediction methods[13,14] used today are based on semi-empirical methods. In these methods, characteristic length and velocity scales are usually determined from curve fits obtained from experiments or flight measurements. In recent years, Computational Aeroacoustics (CAA) methods[15] have been used to simulate acoustic scattering from trailing edges. These methods couple time-accurate flow field data obtained from RANS or Large Eddy Simulation solutions with acoustic equations to propagate the noise to the far-field. They can give accurate results, however they are restricted to simple problems due to the computational expense stemming from the very fine time and space resolution requirements. For our problem, considering the geometry of interest and the number of runs to be performed for creating response surfaces, it is impractical to use Computational Aeroacoustics . However, we still perform 3-D, steady-state (non-time-accurate), RANS simulations to calculate the characteristic velocity and length scales.

### Derivation of the Noise Metric

Following the approach by Goldstein[8] and Lilley,[5,9] one can approximate the far-field noise intensity per unit volume of acoustic sources at the trailing edge of a wing surface as

$$I \approx \frac{\rho_\infty}{2\pi^3 a_\infty^2}\omega_0 u_0^4 Cos^3\beta \frac{D(\theta,\psi)}{H^2}, \qquad (1)$$

where $\rho_\infty$ is the free-stream density, $a_\infty$ is the free-stream speed of sound, $\omega_0$ is the characteristic source frequency, $u_0$ is the characteristic velocity scale for turbulence, $H$ is the distance to the ground (receiver) and $\beta$ is the trailing edge sweep angle. Lilley[5] gives a simplified version of Equation 1 for the flyover case with a polar directivity angle ($\theta$) of 90° which makes the directivity term $D(\theta,\psi)$ equal to unity. He also neglects the $Cos^3\beta$ term given by Howe[10] since the contribution of this term is small for most conventional wings. However, this term also shows that the radiated noise from scattering may be reduced to a smaller value for wings with highly swept trailing edges. We write Equation 1 for any wing configuration and receiver position. We do not include the Doppler factors due to convection of acoustic sources, since we focus on low Mach numbers which are between 0.2 and 0.3 for typical aircraft at approach before landing. The directivity term is in the form given by Ffowcs-Williams and Hall:[12]

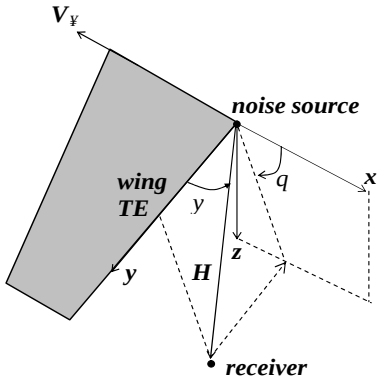


Figure 2: **Directivity angles used in the noise metric (note that the trailing edge sweep angle ($\beta$) is 0° in this figure)**

$$D(\theta,\psi) = 2Sin^2(\frac{\theta}{2})Sin\psi. \qquad (2)$$

Here, $\theta$ is the polar directivity angle and $\psi$ is the azimuthal directivity angle. (Figure 2). Using the Strouhal relation for turbulent flow,[5]

$$\frac{w_0 l_0}{u_0} \approx const. \qquad (3)$$

one can re-write Equation 1 with the characteristic length scale for turbulence $l_0$:

$$I \approx \frac{\rho_\infty}{2\pi^3 a_\infty^2} u_0^5 l_0^{-1} Cos^3\beta \frac{D(\theta,\psi)}{H^2}. \qquad (4)$$

Since we would like to design a wing for minimum noise, we consider the spanwise variation of the characteristic velocity, characteristic length scale, the trailing edge sweep, the directivity angles, and the distance to the receiver point (i.e., $u_0 = u_0(y)$,

$l_0 = l_0(y)$, $\beta = \beta(y)$, $\theta = \theta(y)$, $\psi = \psi(y)$, and $H = H(y)$). We have seen the importance of retaining the spanwise variation of the characteristic velocity and length scale in our three-dimensional parametric study, since the change in these variables was significant along the span at higher lift coefficients. Assuming a correlation volume per unit span at the trailing edge as

$$dV = l_0^2 dy, \tag{5}$$

Equation 4 can be written for the correlation volume given above and integrated over the span $b$ to obtain

$$I_{NM} = \frac{\rho_\infty}{2\pi^3 a_\infty^2} \int_0^b u_0^5 l_0 Cos^3\beta \frac{D(\theta,\psi)}{H^2} dy, \tag{6}$$

where $I_{NM}$ is the noise intensity indicator which can be evaluated on the upper or the lower surface of the wing. Note that $I_{NM}$ is not the absolute value of noise intensity, however we expect it to be an accurate indicator as a relative noise measure. We scale $I_{NM}$ with the reference noise intensity of $10^{-12}\ W/m^2$ (the minimum sound intensity level that human ear can detect) which is a common practice in acoustics. Finally, we write the Noise Metric ($NM$) for the trailing edge noise (in dB) as:

$$NM = 120 + 10log\left(I_{NM}\right). \tag{7}$$

To obtain the total noise metric for a wing, we calculate the noise metric values for the upper ($NM_{upper}$) and the lower surfaces ($NM_{lower}$), and add them as

$$NM = 10log\left(10^{\frac{NM_{upper}}{10}} + 10^{\frac{NM_{lower}}{10}}\right). \tag{8}$$

**Modeling of $u_0$ and $l_0$**

In the noise metric, the characteristic turbulent velocity at a spanwise location of the wing trailing edge can be chosen as the maximum value of the turbulent kinetic energy ($TKE$) profile at that particular spanwise station:

$$u_0(y) = Max\left[\sqrt{TKE(z)}\right]. \tag{9}$$

Here, $z$ is the direction normal to the wing surface. We model the characteristic turbulence length scale for each spanwise station as:

$$l_0(y) = \frac{Max\left[\sqrt{TKE(z)}\right]}{\omega}. \tag{10}$$

In Equation 10, $\omega$ is the turbulence frequency (dissipation rate per unit kinetic energy) observed at the maximum $TKE$ location. We view this choice of a turbulence length scale as more soundly based than other suggestions in the literature like the boundary layer thickness or the displacement thickness. These lengths are related to the mean flow and do not reflect anything about the turbulence structure. We obtain $TKE$ and $\omega$ from the solutions of the $TKE$-$\omega$ ($k$-$\omega$) turbulence model equations used in the Navier-Stokes calculations.

## CFD Simulations

The CFD code GASP[16] has been used for physical modeling of all validation and parametric noise metric cases presented in this paper. GASP is a three-dimensional, structured, multi-block, finite volume, Reynolds-Averaged Navier-Stokes (RANS) code. In the CFD simulations, inviscid fluxes were calculated by an upwind-biased third-order spatially accurate Roe flux scheme. Asymptotic convergence to a steady state solution was obtained for each case. The iterative convergence of each solution was examined by monitoring the overall residual, which is the sum (over all the cells in the computational domain) of the $L^2$ norm of all the governing equations solved in each cell. In addition to this overall residual information, some of the output quantities such as the lift coefficient and the $TKE$ distributions were also monitored. Each case was run at three grid levels: coarse, medium, and fine. Medium and coarse grid levels were obtained from the fine grid by reducing the number of grid points by a factor of two at each direction. At each grid level, except the coarsest one, the initial solution estimates were obtained by interpolating the primitive variable values of the previous grid solution to the new cell locations. This method, known as grid sequencing, was used to reduce the number of iterations required to converge to a steady state solution at finer mesh levels. All the results presented in this paper were obtained with the finest mesh level. Coarse, medium, and fine grid levels were used to check the grid convergence. In the CFD simulations, we solved full Navier-Stokes equations by including all the viscous terms in the physical model. All the runs were made with the assumption of fully-turbulent flow. Menter's $k$-$\omega$ SST turbulence model[17] was used in all the calculations. This model has been shown[18] to give better overall accuracy in different types of flows compared to the other two-equation turbulence models.

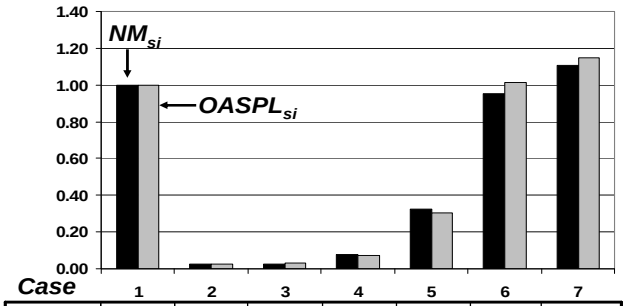


| Case | 1 | 2 | 3 | 4 | 5 | 6 | 7 |
|---|---|---|---|---|---|---|---|
| $\alpha$ (deg) | 0.0 | 0.0 | 2.0 | 1.5 | 0.0 | 2.0 | 1.5 |
| $Re_c x10^{-6}$ | 1.497 | 0.665 | 0.499 | 0.831 | 1.164 | 1.122 | 1.497 |

Figure 3: **The comparison of scaled predicted noise metric value ($NM_{si}$) to the scaled experimental OASPL[14] ($OASPL_{si}$) at each NACA 0012 validation case**

## Noise Metric Validation

Noise metric validation was performed with seven test cases shown in Figure 3. These cases were selected from a two-dimensional NACA 0012 experimental database. To create this database, Brooks *et al.*[14] conducted experiments at different speeds, angles of attack, and chord lengths using NACA 0012 airfoils and measured the 1/3-octave Sound Pressure Level (SPL) spectra of the noise generated by the airfoils. They also used this database to develop a semi-empirical airfoil self-noise prediction method. The SPL spectrum of each case was measured at a point 1.22 m away from the mid-span trailing edge. Both directivity angles $\theta$ and $\psi$ were 90° at this location.

The main noise mechanism of all the cases used in the validation study is the trailing edge noise generated by the scattering of turbulent pressure fluctuations over the trailing edge. These cases were chosen to cover a wide range of speeds (71.3, 55.5, 39.6, and 31.7 m/s) at different angles of attack. The difference between the Reynolds number of each case shown in Figure 3 is due to the change in speed. All the other flow conditions were kept constant and the chord length of the airfoil was the same (0.3048 m).

CFD simulations were performed for each noise metric validation case. The noise metric of each case, $NM_i$, was calculated using the characteristic velocity and the length scales obtained from the CFD simulations in Equation 8 with Equations 9 and 10. For the same cases, the Overall Sound Pressure Levels ($OASPL_i$) were calculated from the experimental data. The noise metric for each case was scaled with the value obtained for Case 1:

$$NM_{si} = 10^{[0.1(NM_i - NM_1)]} \tag{11}$$

A similar scaling was done for the OASPL values:

$$OASPL_{si} = 10^{[0.1(OASPL_i - OASPL_1)]} \tag{12}$$

Figure 3 shows the comparison of $NM_{si}$ and $OASPL_{si}$ at each case. As can be seen from this figure, the agreement between the experiment and our predictions are very good at various speeds and angles of attack. This figure also demonstrates that the noise metric is capable of capturing the variations in the trailing edge noise as a relative noise measure when different flow conditions and parameters are changed.

## Parametric Noise Metric Studies

Parametric studies to investigate the effect of the wing geometry and the lift coefficient on the noise metric were performed. Two-dimensional parametric studies were done using two subsonic (NACA 0012 and NACA 0009) and two supercritical (SC(2)-0710 and SC(2)-0714) airfoils. A generic conventional transport wing was used for the three-dimensional study.

The influence of the flight speed on the trailing edge noise is well-known, since the noise is proportional to the $5^{th}$ power of the velocity as shown by all the aeroacoustic theories on this subject. We include this effect in our noise metric since the characteristic velocity $u_0$ will change in proportion to the free-stream velocity in most cases. In addition to the speed, one also would like to know the effect of the other variables such as the lift coefficient and the wing geometry on the trailing edge noise. The information obtained from the parametric studies will be useful in our MDO studies, since it will help to select the appropriate design parameters in the optimization process. The main results obtained from these cases are presented and discussed in the following two sections.

### Two-Dimensional Studies

#### NACA 0009 and NACA 0012 airfoils

The main purpose of the study with NACA 0012 and NACA 0009 airfoils was to investigate the noise reduction by changing the lift coefficient and the thickness ratio. To study this objective, the lift coefficient was reduced while increasing the chord length to have the same lift at a constant speed. Further reduction was sought by decreasing the thickness ratio. This 2-D study can be thought of as a simplified representation of increasing the wing area and reducing the overall lift coefficient of an aircraft at constant

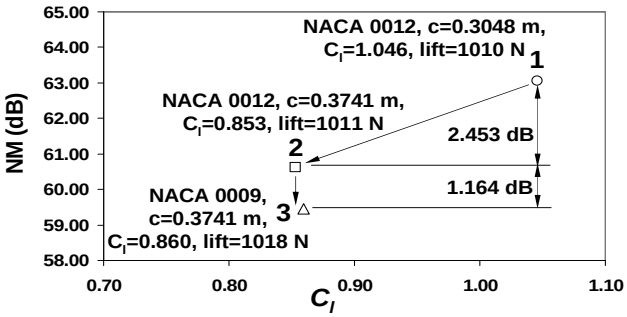


Figure 4: **Noise metric reduction history obtained with NACA 0012 and NACA 0009 airfoils for various lift coefficients at constant lift**

lift and speed. As part of this study, three configurations were considered: (1) NACA 0012 airfoil with a chord length of 0.3048 m, (2) NACA 0012 airfoil with a chord length of 0.3741 m, and (3) NACA 0009 airfoil with a chord length of 0.3741 m. All cases were run with a free-stream velocity ($V_\infty$) of 71.3 m/s and a Mach number of 0.2. The Reynolds number based on the chord ($Re_c$) was $1.497 \times 10^6$ for Case 1 and $1.837 \times 10^6$ for the other two cases. CFD simulations were performed for each case. Computational grids had C-topologies, each having 388 cell centers in the streamwise direction and 64 points in the normal direction to the airfoil surface. The noise metric was calculated at a distance ($H$) 1.22 m away from the trailing edge with the directivity angles $\theta = 90°$ and $\psi = 90°$ (the same values used in the validation studies). Note that these values are arbitrary since we are interested in the relative change of the noise metric and we assume that the receiver is at the same location for all the cases.

Figure 4 shows the noise reduction history of this study. We started from Case 1 with the NACA 0012 airfoil at a lift coefficient ($C_l$) of 1.046. $C_l$ was reduced to 0.853 at Case 2 while increasing the chord length by 23% to keep the lift at a constant value of approximately 1010 Newtons. A noise reduction of 2.45 dB was achieved between Case 1 and Case 2. When the thickness of the airfoil was decreased by 25% (NACA 0009) while keeping the same chord length and the lift, we got an additional reduction of 1.16 dB in the noise metric. Total noise reduction was 3.61 dB . Decreasing the lift coefficient contributed 68% of the total noise reduction.

This simple example showed that it is possible to reduce the trailing-edge noise by increasing the chord length (wing area) and decreasing the lift coefficient and the thickness ratio. Another benefit from this approach can come from eliminating the need to use high-lift devices which are the dominant airframe noise sources on approach. If sufficient lift can be obtained with an increased wing area without using high-lift devices, a significant reduction in noise may be achieved. However all these changes should be performed in an MDO framework to account for the other aircraft design requirements.

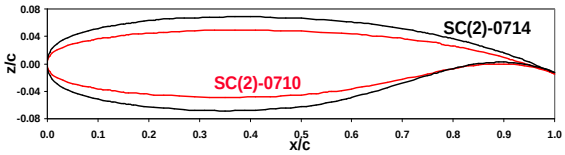


Figure 5: **SC(2)-0710 and SC(2)-0714 airfoils**

## SC(2)-0710 and SC(2)-0714 airfoils

In addition to the NACA four digit airfoil cases, two-dimensional parametric studies were performed with supercritical airfoils at realistic flight conditions to study the effect of the lift coefficient and the thickness ratio on the noise metric. We used two supercritical airfoils, SC(2)-0710 and SC(2)-0714 (Figure 5). These airfoils belong to the same family, but have different thickness ratios[19] ($t/c = 10\%$ for SC(2)-0710 and $t/c = 14\%$ for SC(2)-0714). CFD simulations were performed at $Re_c = 44 \times 10^6$ with $V_\infty = 68$ m/s and $Mach = 0.2$. These values approximately correspond to the conditions of a typical transport aircraft having a mean aerodynamic chord ($mac$) of 9.54 m at an altitude of 120 m before landing. At this location, the aircraft is approximately above the point where the noise certification measurements at approach (2000 m away from touchdown point on the runway) are taken.[5] Airfoil grids used in the CFD calculations had $388 \times 64$ cells. The noise metric values were calculated for $H = 120$ m, $\theta = 90°$, and $\psi = 90°$. Figure 6 shows the section lift coefficients obtained at different angles of attack for the two airfoils. For each airfoil, the angle of attack was

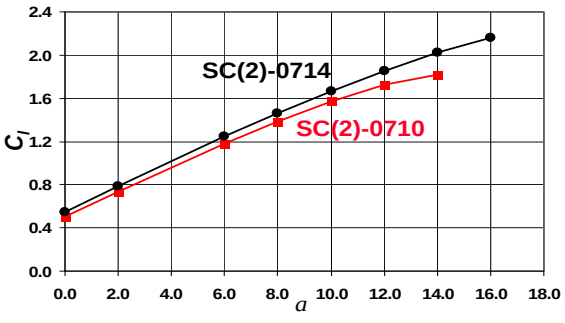


Figure 6: **Section lift coefficient ($C_l$) vs. angle of attack ($\alpha$) for SC(2)-0710 and SC(2)-0714 airfoils**

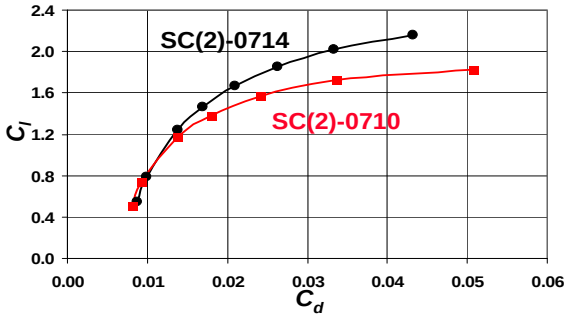


Figure 7: **Drag Polars for SC(2)-0710 and SC(2)-0714 airfoils**

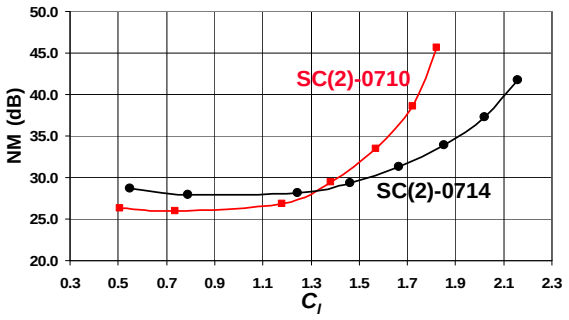


Figure 8: **Noise metric values obtained with SC(2)-0710 and SC(2)-0714 airfoils at different section lift coefficients**

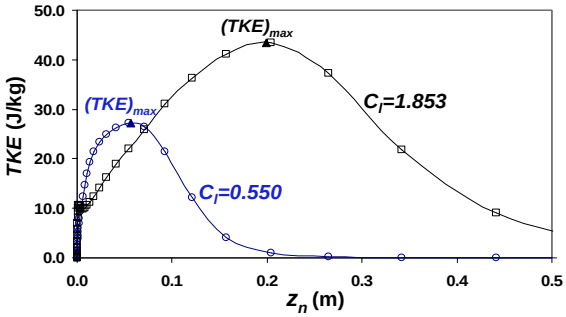


Figure 9: **Turbulent Kinetic Energy ($TKE$) profiles at the upper surface trailing edge of SC(2)-0714 airfoil for $C_l = 0.550$ and $C_l = 1.853$. $z_n$ is the normal distance from the airfoil surface**

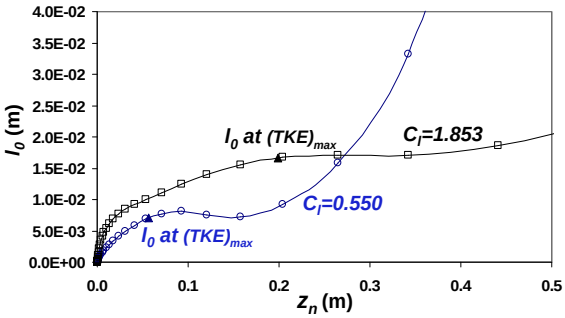


Figure 10: **Characteristic length scale ($l_0$) profiles at the upper surface trailing edge of SC(2)-0714 airfoil for $C_l = 0.550$ and $C_l = 1.853$**

increased to get the highest lift coefficient before stall. As can be seen from this figure, SC(2)-0710, the airfoil with the smaller thickness ratio has a lower maximum $C_l$ value compared to the SC(2)-0714 airfoil. The drag polars for each airfoil are shown in Figure 7. For lift coefficients greater than 0.8, the drag of the SC(2)-0710 airfoil is larger at the same lift. Looking at the noise metric values (Figure 8), we see that the noise of each airfoil stays approximately constant up to a certain lift coefficient value. At this range of lower $C_l$, the thicker airfoil has higher noise metric values. The difference is approximately 2 dB at $C_l = 0.7$. A dramatic increase in the noise metric value can be observed for each airfoil at higher lift coefficients. The large increase in the noise metric at high lift coefficients originates from the increase of both the maximum $TKE$ and the characteristic length scale $l_0$. Figure 9 shows the $TKE$ profiles at the upper surface trailing edge of the SC(2)-0714 airfoil at two $C_l$ values. The significant difference between the maximum $TKE$ values can be seen. A similar observation can be made for the length scale (Figure 10). At high lift coefficients, the adverse pressure gradient close to the upper surface trailing edge increases the thickness of the turbulent boundary layer and the magnitude of the turbulent fluctuations. These values become larger as the flow gets closer to separation.

Figure 8 shows another important effect of the thickness ratio on the noise metric. The noise from the SC(2)-0710 airfoil is larger than the noise of the thicker airfoil at $C_l > 1.35$. This implies that reducing the thickness ratio may in fact increase the noise at higher lift coefficients.

## Three-Dimensional Study

The objective of the three-dimensional study was to examine the effect of the overall lift coefficient $C_L$ on the *clean* wing airframe noise by using a realistic wing geometry at realistic conditions. This study also permitted investigation of the spanwise variation of the characteristic velocity and length scale as the lift coefficient was changed.

The geometry used in this study is the Energy-Efficient Transport (EET) Wing.[20] This is a generic conventional transport aircraft wing (Figure 11) used in many experimental studies at NASA. For our study, we scaled the original dimensions of the experimental model so that the mean aerodynamic chord is 9.54 m. The scaled wing has a reference area ($S_{ref}$)

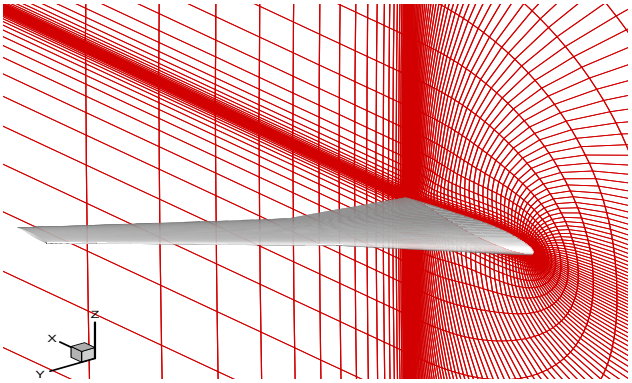

Figure 11: **A view of the EET Wing and the C grid around the root section**

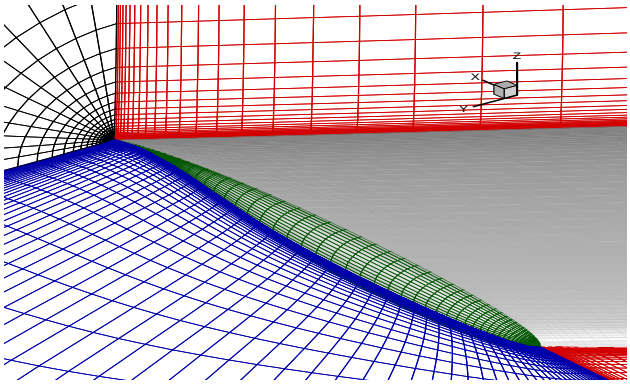

Figure 12: **A view of the EET Wing tip region**

of 511 $m^2$ (based on the wing planform including the leading-edge and trailing-edge extensions of the inboard section) and a span of 64.4 m. It has an aspect ratio of 8.16, a dihedral angle of 5°, and a sweep angle of 30° at the quarter chord. The outboard section of the wing starts at $2y/b = 0.375$. Wing sections are supercritical airfoils with $t/c = 14\%$ at the root, $t/c = 12\%$ at the break point, and $t/c = 10\%$ at the tip. The computational grid used in the CFD simulations has a C-O topology consisting of four blocks with a total number of 884,736 cells (Figures 11 and 12).

For the CFD simulations and the noise metric calculations, the same flow parameters given in the previous section were used. These correspond to the approach conditions of a typical transport aircraft ($Re_{mac} = 44 \times 10^6$, $V_\infty = 68$ m/s, and $Mach = 0.2$). We evaluate the noise metric at an altitude of 120 m, for an observer at the ground level directly below the aircraft which corresponds to $\theta = 90°$ at $y = 0$ plane (see Figure 2). The azimuthal angle $\psi$ is calculated at each spanwise station, however the effect of the change in $\psi$ along the span is negligible.

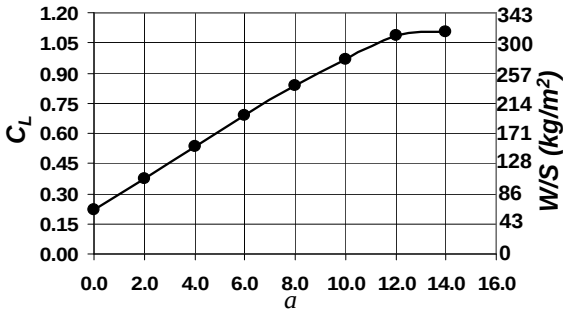


Figure 13: **Overall lift coefficient ($C_L$) and Wing Loading ($W/S$) vs. angle of attack ($\alpha$) for the EET Wing**

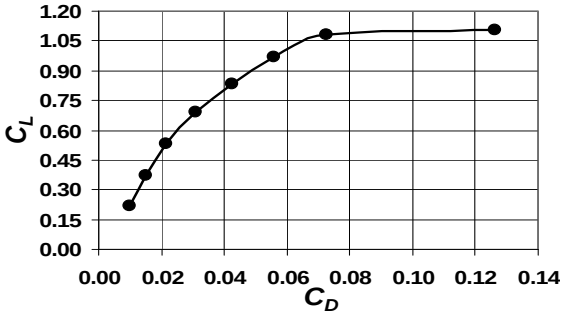


Figure 14: **Drag Polar for the EET Wing**

EET Wing calculations were performed at eight different angles of attack ranging from 0° to 14° with increments of 2°. Figure 13 shows the lift coefficients and corresponding wing loading ($W/S$) values obtained at each angle of attack. The $C_L$ vs. $\alpha$ curve is linear up to 12° where $C_L = 1.084$. At the last angle of attack, one can see the break of the linear pattern which indicates stall. This can also be seen from the drag polar given in Figure 14. The sharp increase in drag at the last angle of attack, where $C_L = 1.106$, is due to a large flow separation on the wing. With this wing configuration, the highest wing loading value that could be achieved was 315.7 $kg/m^2$ (64.8 $lb/ft^2$). On the other hand, for a $B$-777 like transport aircraft, we find that $W/S$ is approximately 432 $kg/m^2$ (88.8 $lb/ft^2$) when using the maximum design landing weight of such an aircraft and $S_{ref}$ of our wing. Although one can reach relatively high lift coefficients with a clean wing by increasing the angle of attack without having substantial separation, it is clear that it would be almost impossible to achieve the lift required to sustain a conventional aircraft at the approach without using high-lift devices. This again shows the importance of having a large wing area to reduce the wing loading at a constant speed, if one wants to design a clean wing at approach conditions that will fly with a low

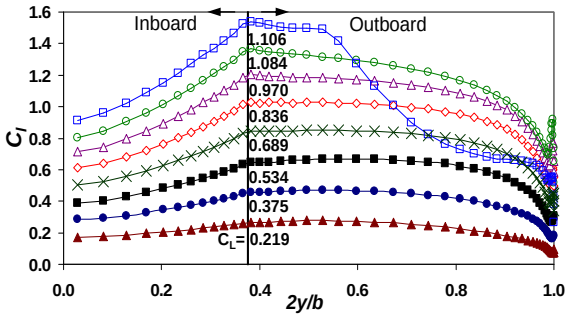


Figure 15: **Section lift coefficient distributions for the EET Wing**

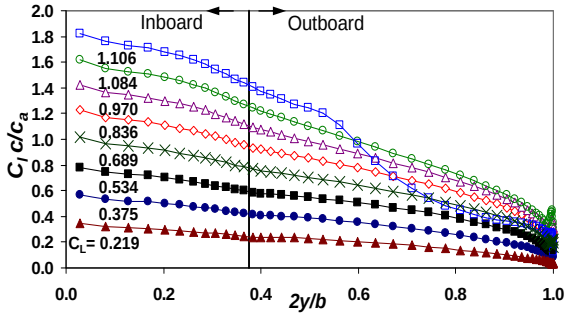


Figure 16: **Spanload distributions for the EET Wing**

lift coefficient to give the minimum noise signature.

The section lift coefficient ($C_l$) and the spanload distributions are given in Figures 15 and 16. The spanload and the $C_l$ exhibit smooth variations along the half-span for all $C_L$ except the highest value. At this lift coefficient, a large loss in lift on the outboard section of the wing starting from $2y/b \approx 0.6$ can be seen. The large separation on the outboard section of the wing at $C_L = 1.106$ is visible in Figure 17 which shows the skin-friction ($c_f$) contours of wing upper surface at four lift coefficients. For $C_L = 0.375$ and 0.689, the skin-friction lines show a smooth pattern along the span except the small kink at the break point. At $C_L = 0.970$ which corresponds to $\alpha = 10°$, a large separation is not observed, but small separated flow regions close to the trailing edge along the span, which can increase the $TKE$ and length scale $l_0$, can be seen.

In fact, looking at the maximum TKE (Figure 18) and the $l_0$ (Figure 19) distributions along the span, we see this increase starting at $C_L = 0.836$ especially on the outboard section of the wing where the section lift coefficients are higher. At the highest lift coefficient, a large increase in the maximum $TKE$ and $l_0$ at the trailing edge of the outboard section where there is massive separation is observed. The change in $TKE$ and $l_0$ is small along the span at

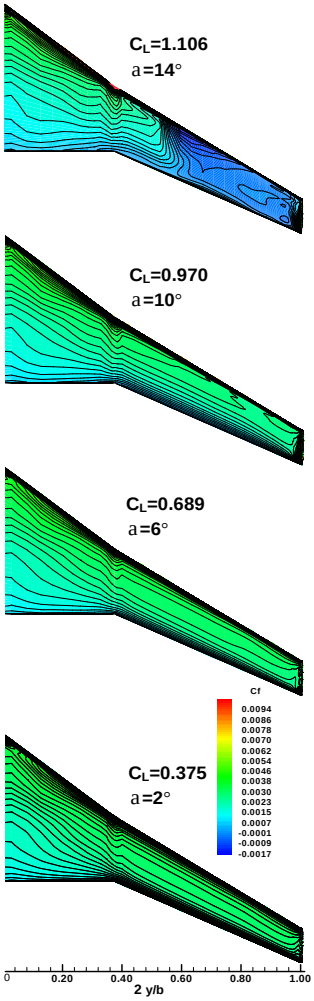


Figure 17: **Skin friction contours of the EET Wing upper surface at different $C_L$ values**

lower lift coefficients ($C_L < 0.836$), except for the tip region where we see the effect of the tip vortex and an increase in $TKE$ (Figure 20). The tip vortex region is small at moderate angles of attack and does not have a significant effect on the overall noise metric. At higher lift coefficient values ($C_L > 0.836$), the maximum $TKE$ and $l_0$ are not uniform along the span, and they get larger at outboard sections due to three-dimensional effects. This shows the importance of calculating the noise metric, especially at high lift coefficients, with a characteristic velocity and length scale that vary along the span.

The noise metric results for the EET Wing are given in Figure 21. At lower lift coefficient values, the noise metric remains approximately constant. The contribution to the total noise from the lower surface is significant at these low $C_L$ values. As we increase the lift coefficient, the upper surface starts to

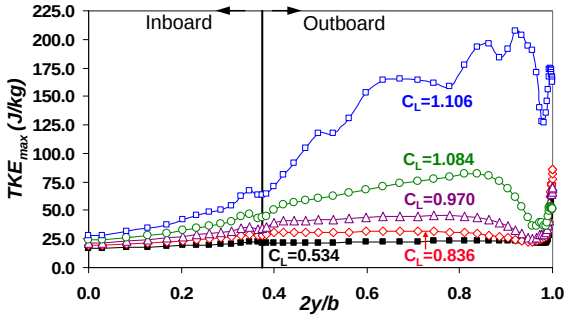


Figure 18: **Maximum $TKE$ distributions along the upper surface trailing edge of the EET Wing**

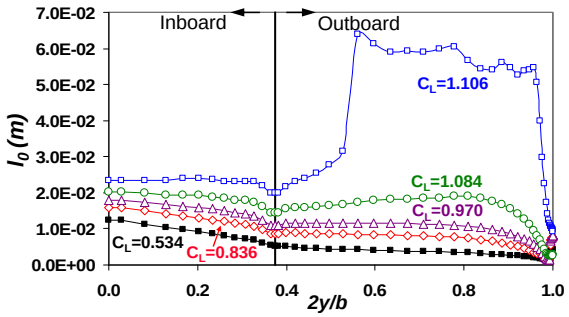


Figure 19: **Characteristic length scale ($l_0$) distributions along the upper surface trailing edge of the EET Wing**

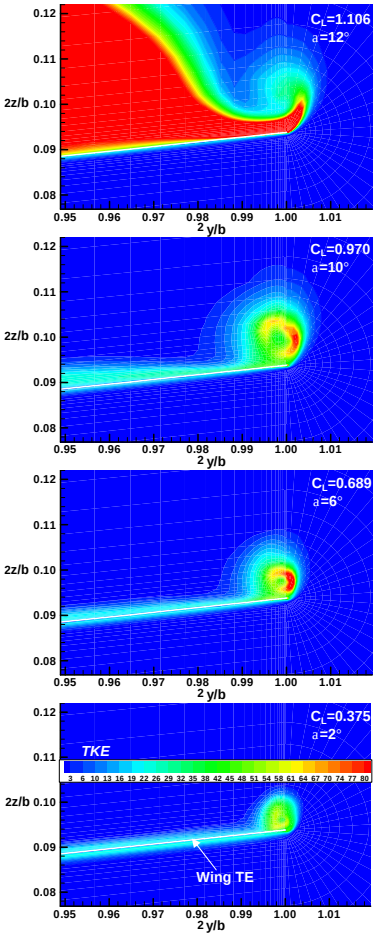


Figure 20: **Turbulent Kinetic Energy contours in the vicinity of the EET Wing tip trailing edge region (looking from downstream) at different $C_L$ values. Note that the maximum TKE of the last case ($C_L$ = 1.106) is much greater than the contour upper limit.**

dominate the noise and the noise metric gets larger. We can see a 15 dB difference in the noise between $C_L = 0.219$ and $C_L = 1.084$. At the highest lift coefficient, a dramatic increase in the noise metric due to the flow separation can be noticed.

The above results suggest that the twist distribution, especially at the outboard section of the wing, may play an important role in the reduction of the trailing edge noise at high lift coefficients. Our current work includes finding the optimum twist distribution for minimum noise. By modifying the twist on the outboard section of the wing, we seek to lower maximum section lift coefficient values and delay the increase in $TKE$ and $l_0$.

## Conclusions

In this paper, we have focused on the airframe noise modeling of a clean wing at approach conditions. We have developed a new noise metric for constructing response surfaces that may be used in the optimization of a clean wing for minimum noise. Our noise metric is not the absolute value of the noise intensity, however it is expected to be an accurate indicator as a relative trailing-edge noise measure. Our methodology for obtaining a noise metric of a clean wing includes a modified version of the theoretical trailing edge noise prediction models. We use a high fidelity CFD (RANS) code with a two-equation turbulence model to obtain the characteristic velocity and length scales that are used in the noise metric. A length scale directly related to the turbulent structure of the flow at the trailing edge was introduced. We allow the spanwise variation of the characteristic velocity and the length scale in our noise model.

Noise metric validation was performed with seven test cases that were selected from a two-dimensional NACA 0012 experimental database. The agreement between the experiment and our predictions was very good at various speeds and angles of attack, which showed that the noise metric is capable of capturing the variations in the trailing edge noise as a relative

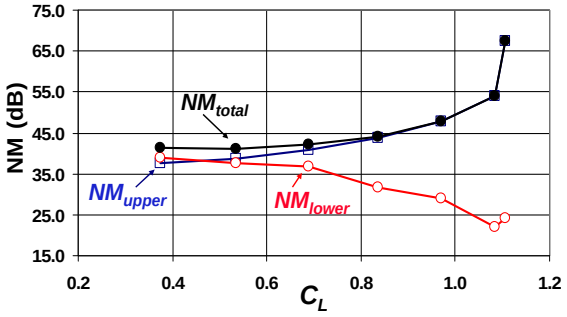


Figure 21: **Noise metric values obtained with the EET Wing at different $C_L$ values**

noise measure when different flow conditions and parameters are changed.

Parametric studies were performed to investigate the effect of the wing geometry and the lift coefficient on the noise metric. Two-dimensional parametric studies were done using two subsonic (NACA 0012 and NACA 0009) and two supercritical (SC(2)-0710 and SC(2)-0714) airfoils. The EET Wing (a generic conventional transport wing) was used for the three-dimensional study. The information obtained from the parametric studies is important for our MDO studies, since it will help to select the appropriate design parameters in the optimization process.

With the NACA 0012 and NACA 0009 airfoils, we were able to show a reduction in the trailing edge noise by decreasing the thickness ratio and the lift coefficient, while increasing the chord length to keep the same lift at a constant speed. This 2-D study can be considered as a simplified representation of increasing the wing area and reducing the overall lift coefficient of an aircraft at constant lift and speed. Another benefit of increasing the wing area may be minimizing or eliminating the need for high-lift devices, which are the dominant airframe noise sources at the approach.

Supercritical airfoil studies showed that decreasing the thickness ratio may increase the noise at high lift coefficients while a reduction may be obtained at low lift coefficients.

Both two- and three-dimensional studies demonstrated that the trailing edge noise remains almost constant at low lift coefficients whereas it gets larger at higher lift coefficients. The increase in the noise metric can be dramatic when there is large flow separation on the wing.

At higher lift coefficient values, the EET wing study showed that maximum $TKE$ and $l_0$ at the trailing edge are not uniform along the span, and they get larger at outboard sections due to three-dimensional effects. This indicates the importance of calculating the noise metric, especially at high lift coefficients, with a characteristic velocity and length scale that vary along the span.

## Acknowledgements

This work is supported by NASA Langley Research Center Grant NAG 1-02024. The authors would like to thank Prof. Raphael T. Haftka (University of Florida) for his helpful comments and suggestions throughout the coarse of this work.

## References

[1] NASA Aeronautics Blueprint: *Toward a Bold New Era in Aviation*. http://www.aerospace.nasa.gov/aero_blueprint/cover.html.

[2] Antoine, N. E. and Kroo, I. M. "Aircarft Optimization For Minimal Environmental Impact", AIAA Paper 2002-5667, September 2002.

[3] Aeronautics and Space Transportation Technology: Three Pillars for Success, *Turning Goals Into Reality*. NASA Annual Progress Report 1997-98.

[4] Crighton, D. G. Airframe Noise (Chapter 7). In *Aeroacoustics of Flight Vehicles: Theory and Practice, Volume 1: Noise Sources*, pages 397–447. edited by Hubbard, H. H., *NASA Reference Publication* 1258, *WRDC Technical Report* 90-3052, 1991.

[5] Lilley, G. M. "The prediction of Airframe Noise and Comparison with Experiment". *Journal of Sound and Vibration*, **239**(4):849–859, 2001.

[6] Ko, A., Leifsson, L. T., Schetz, J. A., Mason, W. H., Grossman, B., and Haftka, R. T. "MDO of a Blended-Wing-Body Transport Aircraft with Distributed Propulsion", AIAA Paper 2003-6732, November 2003.

[7] Dippold, V. F., Hosder, S., and Schetz, J. A. "Analysis of Jet-Wing Distributed Propulsion From Thick Wing Trailing Edges", AIAA Paper 2004-1205, January 2004.

[8] Goldstein, M. E. *Aeroacoustics*. McGraw-Hill Book Company, New York, 1976.

[9] Lilley, G. M. "A Study of the Silent Flight of the Owl", AIAA Paper 1998-2340, 1998.

[10] Howe M. S. "A Review of the Theory of Trailing Edge Noise". *Journal of Sound and Vibration*, **61**(3):437–465, 1978.

[11] Lighthill, M. J. On Sound Generated Aerodynamically. I. General Theory . In *Proceedings of the Royal Society* **A211**, pages 564–587. London, 1952.

[12] Ffowcs Williams, J. E. and Hall, L. H. "Aerodynamic Sound Generation by Turbulent Flow in the Vicinty of a Scattering Half Plane". *Journal of Fluid Mechanics*, **40**(4):657–670, March 1970.

[13] Fink, M. R. Airframe Noise Prediction Method. Report No. FAA-RD-77-29, Federal Aviation Administration, March 1977.

[14] Brooks, T. F., Pope, S. D., and Marcolini, M. A. "Airfoil Self-Noise and Prediction". NASA Reference Publication 1218, NASA Langley Research Center, July 1989.

[15] Singer, B. A., Brentner, K. S., Lockard, D. P., and Lilley, G. M. "Simulation of Acoustic Scattering from a Trailing Edge", AIAA Paper 1999-0231, 1999.

[16] *GASP User Manual*. AeroSoft, Inc., Blacksburg, Virginia, 1997.

[17] Menter F. "Two-Equation Eddy-Viscosity Turbulence Models for Engineering Applications ". *AIAA Journal*, **32**:1598–1605, 1994.

[18] Bardina, J. E., Huang, P. G., and Coakley, T. J. "Turbulence Modeling Validation", AIAA Paper 1997-2121, 1997.

[19] Harris, C. D. "NASA Supercritical Airfoils *A Matrix of Family Related Airfoils*" . NASA Technical Paper 2969, NASA Langley Research Center, 1990.

[20] Jacobs, P. F. and Gloss, B. B. "Longitudinal Aerodynamic Characteristics of a Subsonic, Energy-Efficient Transport Configuration in the National Transonic Facility". NASA Technical Paper 2922, NASA Langley Research Center, 1989.